SANDIA REPORT
SAND2004-5332
Unlimited Release
Printed October 2004

In-Situ Scanning Probe Microscopy of Electrodeposited Nickel

Dean C. Dibble, J.J. Kelly

Prepared by
Sandia National Laboratories
Albuquerque, New Mexico 87185 and Livermore, California 94550

Sandia is a multiprogram laboratory operated by Sandia Corporation,
a Lockheed Martin Company, for the United States Department of Energy's
National Nuclear Security Administration under Contract DE-AC04-94-AL85000.

Sandia National Laboratories

Issued by Sandia National Laboratories, operated for the United States Department of Energy by Sandia Corporation.

Available to DOE and DOE contractors from
U.S. Department of Energy
Office of Scientific and Technical Information
P.O. Box 62
Oak Ridge, TN 37831

Telephone:	(865) 576-8401
Facsimile:	(865) 576-5728
E-Mail:	reports@adonis.osti.gov
Online ordering:	http://www.doe.gov/bridge

Available to the public from
U.S. Department of Commerce
National Technical Information Service
5285 Port Royal Rd
Springfield, VA 22161

Telephone:	(800) 553-6847
Facsimile:	(703) 605-6900
E-Mail:	orders@ntis.fedworld.gov
Online order:	http://www.ntis.gov/help/ordermethods.asp?loc=7-4-0#online

SAND2004-5332
Unlimited Release
Printed October 2004

In-Situ Scanning Probe Microscopy of Electrodeposited Nickel

Dean. C. Dibble, J. J. Kelly
Sandia National Laboratories
P.O. Box 969, MS9161
Livermore, California 94551

Abstract

The performance characteristics and material properties such as stress, microstructure, and composition of nickel coatings and electroformed components can be controlled over a wide range by the addition of small amounts of surface-active compounds to the electroplating bath. Saccharin is one compound that is widely utilized for its ability to reduce tensile stress and refine grain size in electrodeposited nickel. While the effects of saccharin on nickel electrodeposition have been studied by many authors in the past, there is still uncertainty over saccharin's mechanisms of incorporation, stress reduction, and grain refinement. *In-situ* scanning probe microscopy (SPM) is a tool that can be used to directly image the nucleation and growth of thin nickel films at nanometer length scales to help elucidate saccharin's role in the development and evolution of grain structure. In this study, *in-situ* atomic force microscopy (AFM) and scanning tunneling microscopy (STM) techniques are used to investigate the effects of saccharin on the morphological evolution of thin nickel films.

By observing mono-atomic height nickel island growth with and without saccharin present we conclude that saccharin has little effect on the nickel surface mobility during deposition at low overpotentials where the growth occurs in a layer-by-layer mode. Saccharin was imaged on Au(111) terraces as condensed patches without resolved packing structure. AFM measurements of the roughness evolution of nickel films up to 1200 nm thick on polycrystalline gold indicate that saccharin initially increases the roughness and surface skewness of the deposit that at greater thickness becomes smoother than films deposited without saccharin. Faceting of the deposit morphology decreases as saccharin concentration increases even for the thinnest films that have 3-D growth.

Acknowledgments

The authors wish to acknowledge the assistance of Alec Talin for obtaining x-ray diffraction pole figures on electrodeposited nickel films and Nancy Yang for optical microscopy and SEM imaging assistance. Sandia is a multi-program laboratory operated by Sandia Corporation, a Lockheed Martin Company, for the United States Department of Energy under Contract DE-AC04-94AL85000.

Contents

Figures

Tables

Nomenclature

AFM	Atomic Force Microscopy
EC	Electrochemical
ED	Electrodeposited
in-situ	Within the normal process, Latin "in position"
LDRD	Laboratory Directed Research and Development
LIGA	Acronym from German Lithographie, Galvanoformung, Abformung (Lithography, Electroforming, Molding)
PCTFE	PolyChloroTriFluoroEthylene, Kel-F® (3M)
SEM	Scanning Electron Microscopy
SNL	Sandia National Laboratories
SPM	Scanning Probe Microscopy (may be AFM or STM)
STM	Scanning Tunneling Microscopy

Intentionally Left Blank

Introduction

The addition of small amounts of organic materials to electroplating baths is frequently employed to control the material properties of electrodeposited films. For many electroplating chemistries, the mechanism by which an additive changes the stress, microstructure, crystallographic texture, composition, and other properties are not fully understood and thus independent control of these properties is restricted and new additive materials must be developed empirically. In-situ scanning probe techniques allow direct observation of the effects of additives on the nucleation and growth process and can account for the initial substrate conditions and morphology. These observations can be used to help elucidate an additive's operative mechanisms and aid the development of new additive formulations.

Of the many additive materials in common use for nickel electrodeposition, saccharin is unique in its properties and performance. Considerable effort has been devoted to understanding its performance as a grain refining[1] and stress reducing agent[2], and its interaction with other additive materials[3]. Important questions remain concerning the local interaction of saccharin with the surface. For example, the mechanism by which saccharin decreases grain size has been postulated to be by decreasing nickel mobility, blocking charge transfer at the surface, interfering with nickel reduction at specific surface features or crystal planes, or by catalyzing the nucleation of new nickel nuclei[1,4]. In the experimental work described below we focus our attention on this versatile additive.

Experimental Details

For the purpose of studying the interaction of additive materials with an evolving surface during electrodeposition, SPM experiments were optimized for continuous acquisition of images from the same location on a sample surface under stable deposition conditions. The successful adaptation of a commercial scanning probe microscope for stable operation in this manner required a significant experimental effort that is beyond the scope of this report.

Electrodes

Working electrodes were 250 +/-50 nm evaporated Au with approximately 5 nm Cr adhesion layer on fused silica, lithographically patterned to form a 2.0 mm diameter disk and 100 micrometer line leading to external electrical connections as shown in Fig. 1. The use of these patterned electrodes improved the uniformity of the electrodeposit in the area being examined by SPM and decreased the electrochemical response time of the system to changes in electroplating potential. Reference electrodes were miniature Ag/AgCl (World Precision Instruments, Sarasota, FL model DRIREF-2SH) and inserted directly into the cell volume. Potential values are quoted relative to Ag/AgCl and are uncorrected for residual solution resistance. A 0.040 inch thick Pt wire formed in an 11.7 mm diameter circle served as a counter electrode. Imaging and

electrochemical measurements were performed in a custom PCTFE (Kel-F) and viton cell with a solution volume of approximately 0.4 mL. A cross section of this cell and the AFM cantilever mount is shown in Fig. 2.

Working and counter electrodes were cleaned in 70% HNO_3 for 24-48 hours prior to use to remove surface contamination. Additionally, working electrodes for STM imaging were annealed in air with a butane-air flame to increase the size of the Au(111) terraces immediately prior to imaging. Experimental hardware such as viton o-rings that could not be cleaned with nitric acid were cleaned ultrasonically with laboratory detergent (Micro, Cole-Parmer, Vernon Hills, IL) and rinsed with de-ionized water.

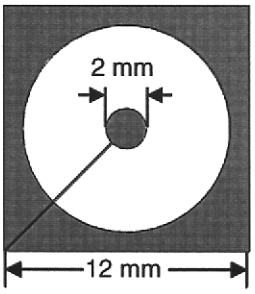

Figure 1. Pattern for working electrodes (cathodes). Grey areas are metalized Au/Cr/SiO_2. The patterning procedure was found to be necessary for experimental consistency.

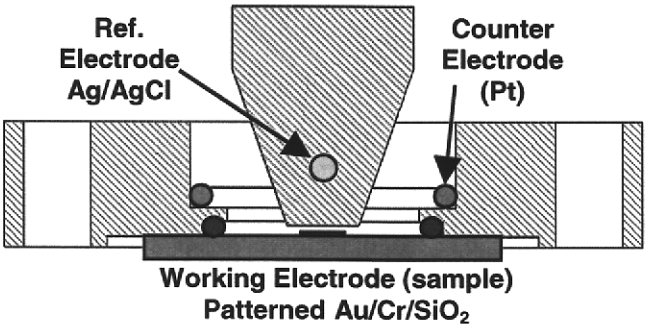

Figure 2. Cross-sectional diagram of experimental SPM cell.

Electroplating Solutions

Four different electroplating solutions were investigated; their compositions are detailed in Table 1 below. Nickel salts and boric acid were Alpha Puratronic grade (99.9985% or better). Saccharin (Aldrich, 99+% as $C_7H_5NO_3S$) or its sodium salt (Alpha, $NaC_7H_4NO_3S$) were present in some of the solutions. Solutions were used as mixed without additional purification or treatment except that all solutions were screened by the 'water break test.' Any solution that produced a hydrophobic reaction—did not wet the surface—of their glass storage bottles was discarded. This rudimentary screening for hydrocarbon contamination appeared to improve the quality of the AFM images acquired. pH of all solutions was 3.9-4.1 as measured with an electronic meter at room

temperature. All experiments were performed at ambient temperature and with solutions exposed to open laboratory air.

Table 1. Composition of experimental solutions.

#	Solution Description	H_3BO_3	$NiSO_4$	$NiCl_2$	Saccharin (sodium salt)	Saccharin
1	Dilute Watts	5×10^{-3} M	1×10^{-2} M	2×10^{-3} M	-	-
2	Dilute Watts, high boric acid	5×10^{-1} M	1×10^{-2} M	2×10^{-3} M	-	-
3	Dilute Watts, high boric acid with low saccharin conc.	5×10^{-1} M	1×10^{-2} M	2×10^{-3} M	-	1×10^{-5} M
4	Dilute Watts, high boric acid with high saccharin conc.	5×10^{-1} M	1×10^{-2} M	2×10^{-3} M	1×10^{-2} M	-

Atomic Force and Scanning Tunneling Microscopy

A Molecular Imaging (Tempe AZ) PicoSPM instrument operating in either constant-force contact AFM or constant current STM mode was used for all experiments. Uncoated silicon probes (type CONT, Nanosensors, Neuschatel Switzerland) held by retaining clips coated with parylene-C reduced stray electrochemical and chemical interactions during AFM imaging. STM imaging was performed with electrochemically etched Pt-Ir tips coated with Shipley Eagle 2100 ED photo-resist (Rohm and Haas, Philadelphia PA). Oven pre-baking resist coated tips to 60° C for 2-4 minutes prior to UV exposure uncovered only a small area of the sharp tips and resulted in a minimum faradic leakage current. All imaging experiments were performed under potentiostatic control.

A total of 19 successful imaging experiments were performed with each producing a sequential set of 25-40 (AFM) or 90-130 (STM) images detailing the evolution of nickel films with or without additives present. For STM imaging, the scan range was chosen to be 400 nm^2 with an image period of 40 seconds for 512 X 512 pixels. STM imaging currents were typically 300-700 pA with tip potential held at or near -0.550 V. Deposits investigated with this imaging mode were typically less then 7 monolayers. AFM images were taken every 256 seconds with a 1 μ^2 area and 512 X 512 pixels at a potential of -0.85 V vs. Ag/AgCl. For these experiments, final nickel film thickness were 300-1200 nm as measured ex-situ with an optical profilometer (Wyco NT3300, Veeco Instruments, Tucson AZ) upon completion of experiments. In most experiments a larger area scan was taken before and after an image series to investigate possible probe artifacts in the scan area. The experiments described here did not appear to produce probe related artifacts at length scales comparable to the scanned area. At larger length scales, however, AFM experiments did produce an enhancement of the growth rate over an area that corresponds to the AFM cantilever and may be due to the conductive silicon material of the cantilever chip as shown in Fig. 3 below. These artifacts appeared to affect film thickness only, no differences in morphology were observed by optical microscopy or under the higher magnification available with SEM.

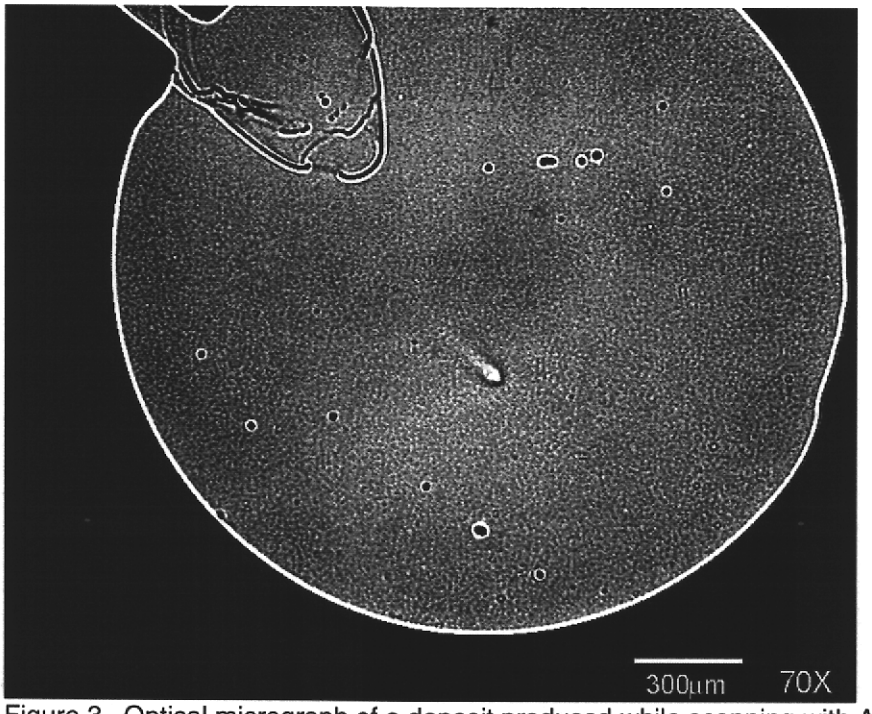

Figure 3. Optical micrograph of a deposit produced while scanning with AFM. A local enhancement of the growth rate was seen in areas near a conductive AFM cantilever. This enhancement was typically less than 10% of the total film thickness.

Image Processing

Raw image processing was performed with SPIP software (Image Metrology A/S, Lyngby Denmark); additional processing and data extraction was accomplished with custom routines written in IDL (Research Systems Inc, Boulder CO). The IDL routines eliminated the apparent image drift by extracting the maximum surface area that was common to the entire image series. The maximum growth rate and current density for our experiments was set such that recognizable surface features could be identified on successive image frames and drift correction algorithms applied successfully.

Results

Electroplating Behavior at low current density and nickel concentration
The choice of electrolyte composition for SPM experiments must be a compromise between competing requirements. A low nickel ion concentration is preferable for studying deposition at growth rates that are slow relative to the scan period of SPM instruments and to access as wide a potential window as possible but must be high enough to prevent depletion of the metal ion within a fixed cell volume. For our experiments the nickel ion concentration was found to be optimal at approximately 10^{-2} M for the study of deposition over a potential range of -0.55V to -0.85V with a maximum current density during imaging of 1 mA/cm^2 as shown in Fig. 4. At this nickel concentration, it was found necessary to maintain a boric acid concentration near the room temperature solubility limit of 0.5 Molar for a uniform and consistent deposit. Boric acid is thought to act as a pH buffer near the cathode surface where there can be a local pH rise due to the co-deposition of hydrogen with nickel. Decreasing the boric acid concentration led to inconsistent results and poor uniformity from the precipitation of $Ni(OH)_2$ at the cathode surface, especially at high growth rates as illustrated by the hull samples in Fig. 5 plated with solutions #1 and #2 from Table 1. The Hull electroplating cell that was used to create these samples maintains a known gradient of current density across the cathode to examine the electroplate appearance over a range of current densities in a single experiment. The sulfate/chloride ratio, pH and 10^{-2} M saccharin concentration were chosen to be typical for LIGA electroforming operations.

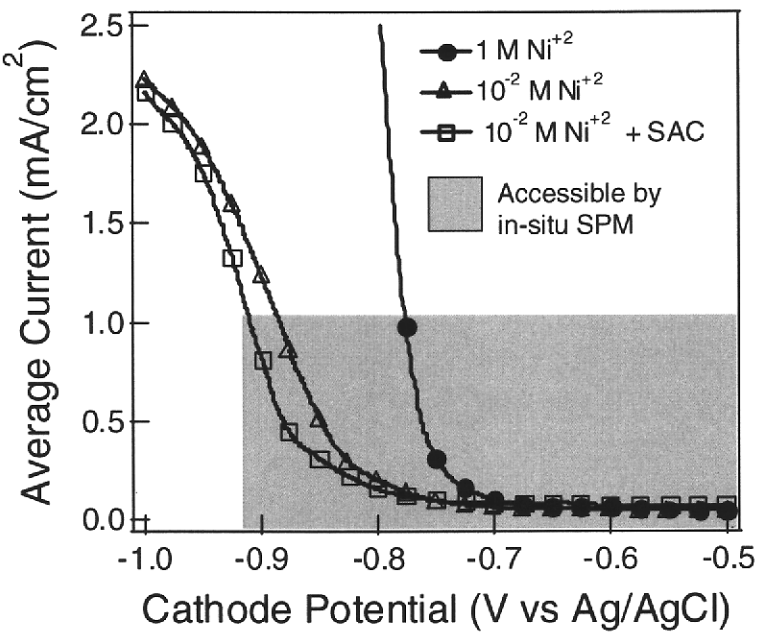

Figure 4. Linear sweep voltamagrams for experimental solutions and for a solution with a concentration typical of LIGA electroforming operations. Reducing the concentration of metal ion in solution allows investigation of a wider potential range when there is an experimental limit on the maximum current density.

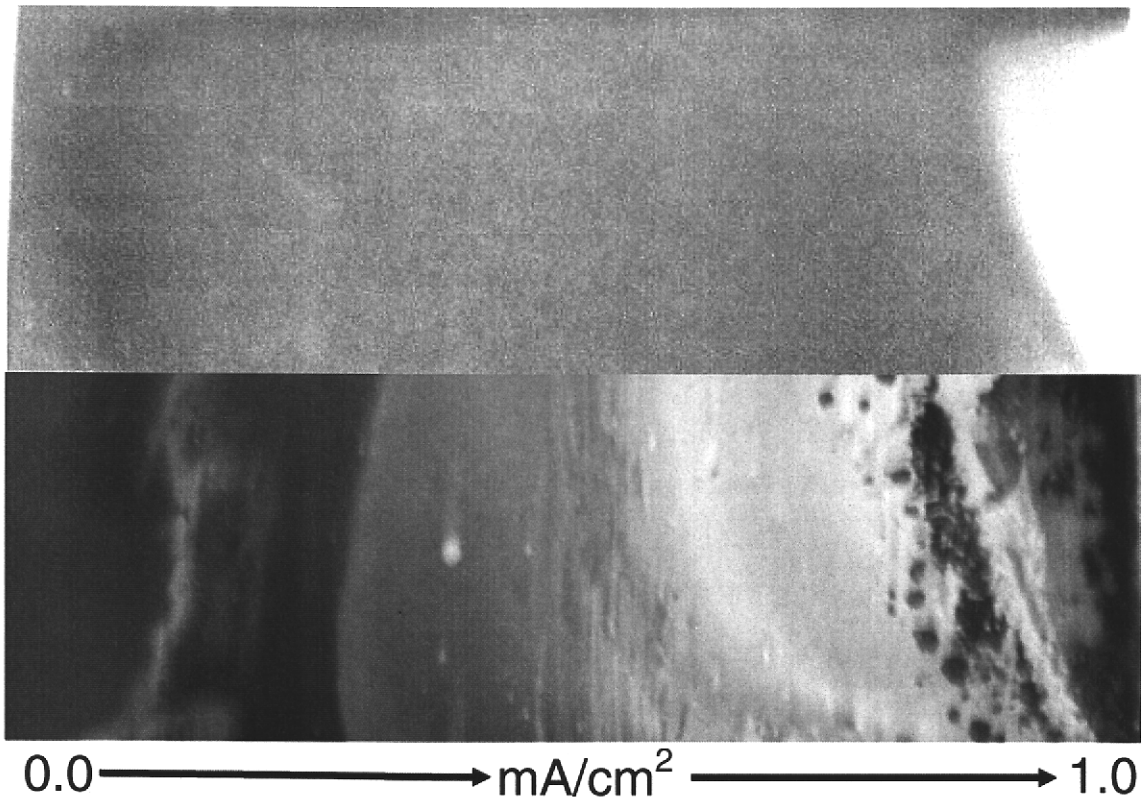

Figure 5. Hull plate samples for different boric acid concentrations. Solution #2 using a boric acid concentration near the saturation concentration of 5 X 10^{-1} M produces a uniform electroplate over a broad current range (top). The boric acid concentration of 5 X 10^{-3} M in solution #1 produces and inconsistent deposit.

Impact of saccharin on nickel surface mobility

Saccharin has been shown previously to cause a decrease in grain size when added to a nickel electroplating bath[1]. One proposed mechanism for this effect is a reduction in mobility of nickel ad-atoms on the cathode surface induced by the presence of saccharin molecules[1]. If this hypothesis is correct, then a reduction in nickel island size or an increase in the disorder of the nickel island perimeters should be apparent when saccharin is included in the electrolyte relative to a saccharin-free deposit produced under identical conditions. In-situ STM possesses sufficient resolution to explore atomically-thin nickel island shapes and determine the effects of saccharin on island morphology.

STM images were recorded during deposition with 0, 10^{-5} M and 10^{-2} M saccharin, i.e. solutions #2-4 from Table 1. Our observations in solutions without saccharin followed closely those published by others despite our use of electrolytes with approximately 50X greater H_3BO_3 and 12X greater Ni ion concentration[5-7]. In our system, nucleation commenced at -0.55 V at the reconstruction elbow sites and at sparse locations at terrace step edges and was followed by growth on the Au(111) terraces at -0.60 V.

The first monolayer of nickel growth indicated a preferred $[1,\bar{1},0]$ growth direction, perpendicular to the double rows of the underlying 'herringbone' reconstruction pattern as shown in Fig. 6a. This first monolayer also possesses a corrugation, or moiré pattern with initial amplitude of 0.06 nm that decreases in succeeding layers. In Fig. 6b it can be seen that the shape of the nickel islands of the 2^{nd}-6^{th} monolayers were considerably more isotropic then in the first monolayer. These layers grew in a layer-by-layer growth mode at the potentials investigated by STM through at least the 6^{th} monolayer.

Repeating this experiment at both 10^{-2} and 10^{-5} M saccharin resulted in a reduction of imaging stability but produced no other significant differences in the nucleation or growth morphology of nickel on Au(111) terraces or step edges through at least the 6^{th} monolayer of nickel as shown in Fig. 7. This suggests that saccharin has only a weak or no effect on the surface mobility of nickel under the conditions examined.

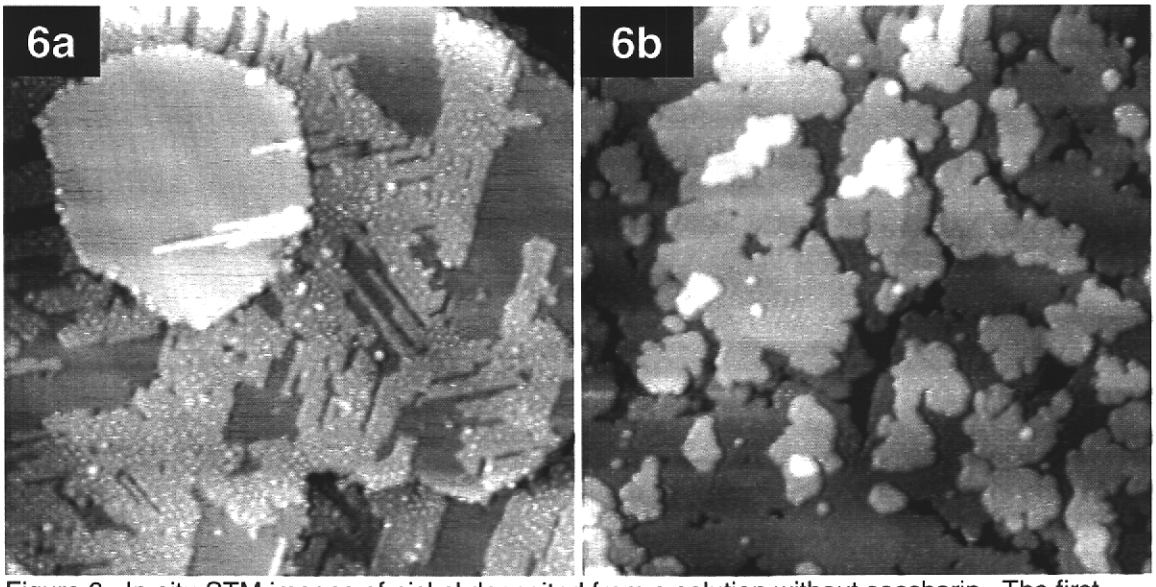

Figure 6. In-situ STM images of nickel deposited from a solution without saccharin. The first monolayer of nickel (a) has a preferred growth direction along the $[1,\bar{1},0]$ direction of the Au(111) surface. By the 5^{th} monolayer (b), the islands have become much more isotropic. 200 X 200 nm STM images.

Imaging of saccharin on Au(111) terraces

At a saccharin concentration of 10^{-5} M, it was possible to image discrete patches of saccharin on bare Au(111) terraces at the onset of nickel deposition. These patches were imaged with an apparent height of just 0.05 nm in the potential range of -0.50 to -0.62 V as shown in Fig. 8. Increasing nickel coverage made the imaging of the thin saccharin layer difficult due to the increased surface roughness and corrugation. At higher saccharin concentrations the saccharin surface coverage approached 100% with only a decrease in imaging stability as an indication that saccharin was present on the surface.

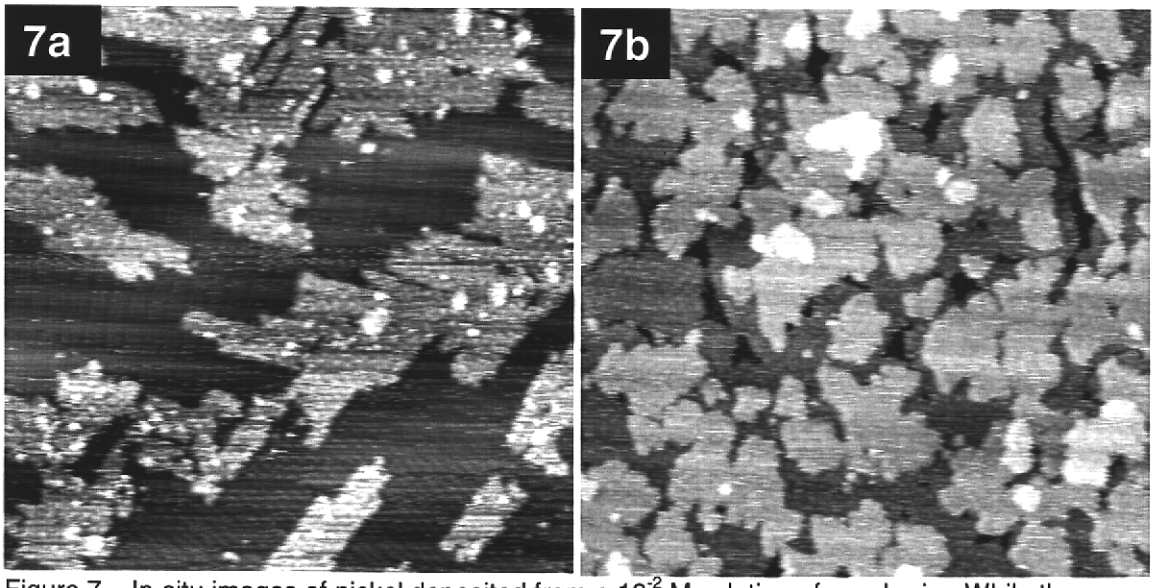

Figure 7. In-situ images of nickel deposited from a 10^{-2} M solution of saccharin. While the stability of imaging is a bit reduced, the preferred growth direction of the first monolayer (a) and the size and shape of the islands on the 5th monolayer (b) are the same as experiments without saccharin. 200 X 200 nm STM image.

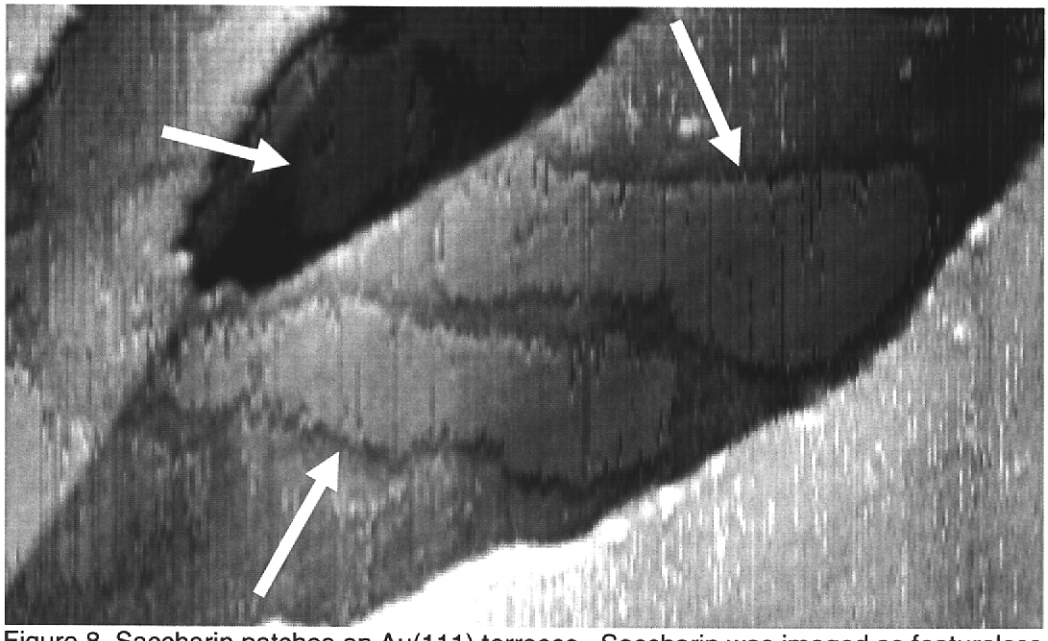

Figure 8. Saccharin patches on Au(111) terraces. Saccharin was imaged as featureless patches (arrows) on Au(111) terraces with a height of 0.05 nm at the onset of nickel deposition. 84 X 141 nm STM image, fast scan direction is top to bottom.

Morphology evolution of electrodeposited nickel

With contact-mode AFM the evolving morphology of the electrodeposit can be followed over length scales and with surface roughness that are much greater than can be probed with STM. At a scale of 1 μm2 the growth and coalescence of 3-D crystallites was followed and the alteration in this behavior induced by saccharin recorded. Two parameters useful for describing the surface at this length scale are the RMS roughness Rq = $\sqrt{\frac{1}{MN}\sum_{j=1}^{N}\sum_{i=1}^{M} z^2(x_j, y_i)}$ for M, N data points in x, y and where z is the surface height relative to the mean surface plane; and surface skewness Rsk = $\frac{1}{MNR_q^3}\sum_{j=1}^{N}\sum_{i=1}^{M} z^3(x_j, y_i)$

Surface skewness is a measure of the asymmetry of the height distribution histogram about its mean. A negative skewness value indicates a predominance of valleys in the surface, positive skewness describes a surface with peaks, and a value of zero indicates the height distribution histogram has a Gaussian distribution.

When saccharin is added to a nickel electroplating solution an initial roughening is induced prior to a net decrease in the roughness relative to a deposit produced without saccharin as shown in Fig. 9. The onset of this initial roughness is also accompanied by a high surface skewness value, indicating that the surface is 'spiky' or 'peaked.' In Fig. 10 the surface skewness is plotted with time for the three saccharin concentrations indicating this initial high skew value with saccharin and also a large negative skew value for deposition without saccharin present during the first approximately 200 nm of nickel growth.

Images of the nickel surface illustrate the difference in morphology induced by the presence of saccharin. Figure 11 presents images taken after 6 minutes of deposition at -0.85 V vs. Ag/AgCl. At this stage of growth the surfaces have a nearly complete coverage of 3-dimensional crystallites with clear differences in morphology for the different saccharin concentrations. With no saccharin in the electrolyte, the crystallites have the appearance of 'hills' or paraboloids with crevices between features. With 10^{-5} M saccharin concentration the first crystallites are much narrower and angular, and in some cases appear to have a triangular aspect. At the higher saccharin concentration of 10^{-2} M there is no indication of faceting on the film and surface features have decreased in size.

Images of thicker deposits at the same locations after 124 minutes in Fig. 12 also display a decrease in feature size with increasing saccharin concentration.

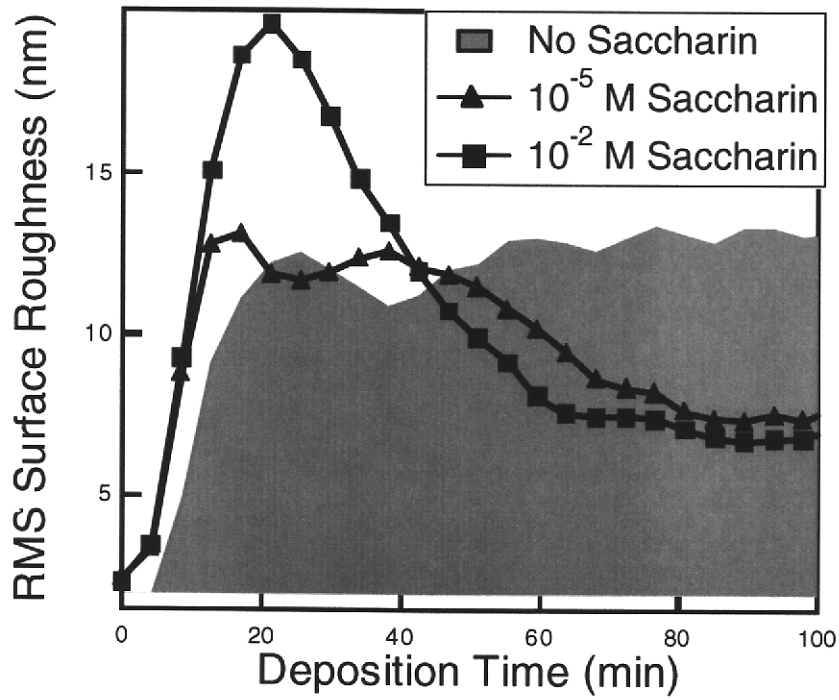

Figure 9. RMS roughness evolution of a 1 μm^2 area for 3 different saccharin concentrations. Saccharin produces an initial increase and then decrease in the roughness of nickel relative to a deposit from a saccharin-free bath.

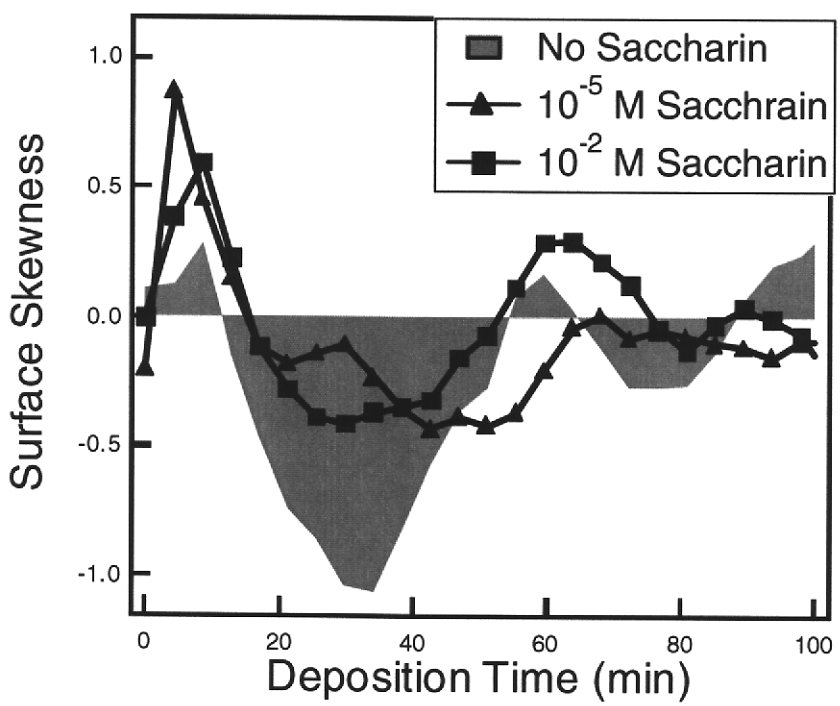

Figure 10. Surface skewness evolution of a 1 μm^2 area for 3 different saccharin concentrations. Saccharin induces a 'peaked' or 'spiky' surface morphology in thin nickel films compared to a 'pitted' or 'creviced' surface produced in the absence of saccharin.

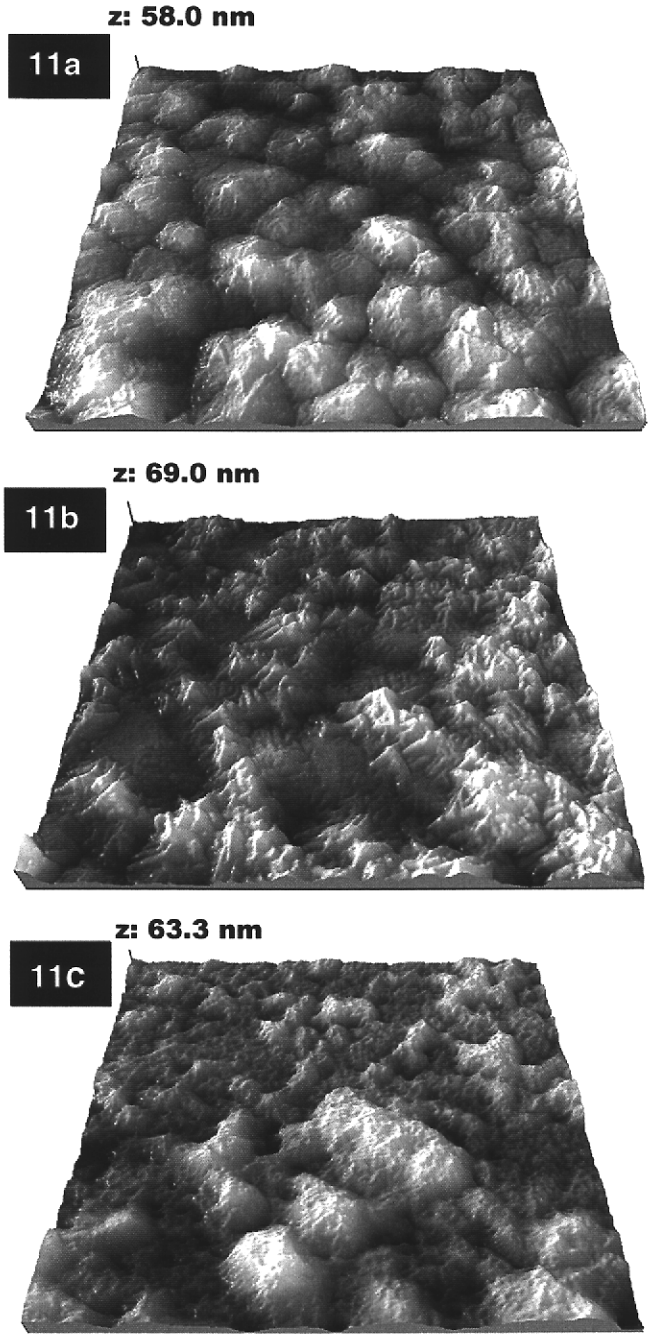

Figure 11. Nickel morphology after 6 minutes of deposition. Saccharin decreases the size and modifies the shape of the initial 3-D crystallites formed on poly-crystalline gold surfaces. Saccharin concentrations are: (a) 0 M, (b) 10^{-5} M, (c) 10^{-2} M. Perspective view AFM images, 1 X 1 μm with the grey z-scale (height) range as indicated on the images.

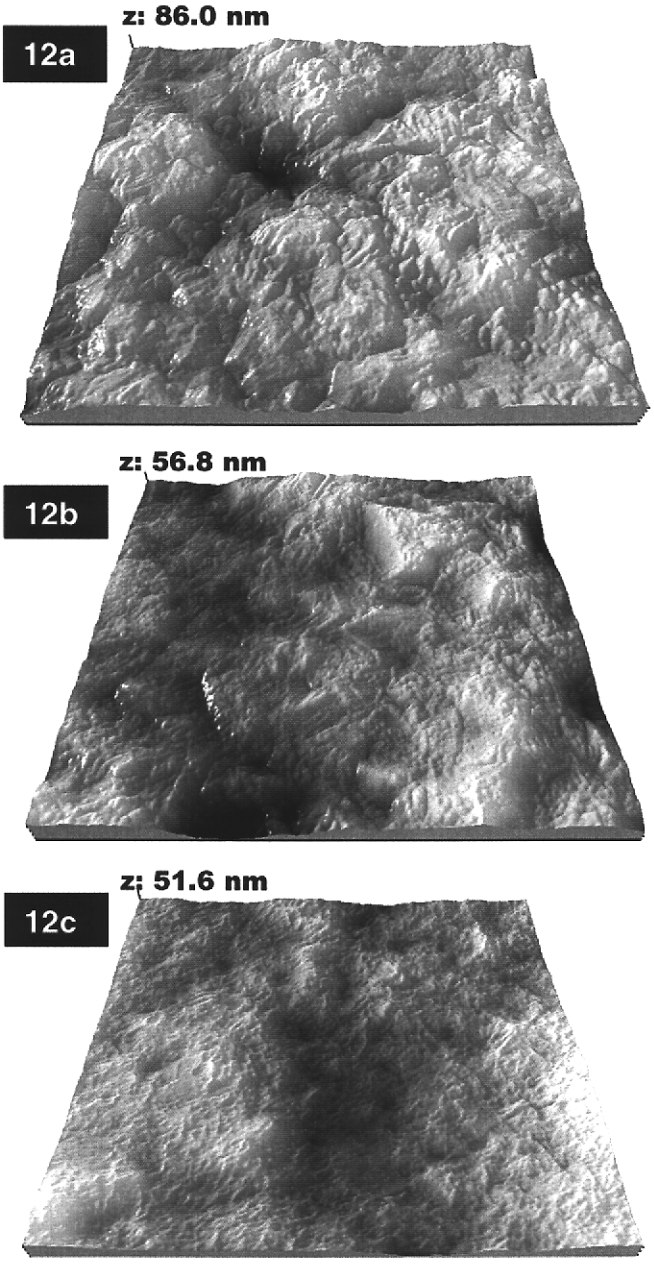

Figure 12. Nickel morphology after 124 minutes of deposition. Features on the surface decrease in size with increasing saccharin concentration. Saccharin concentrations are: (a) 0 M, (b) 10^{-5} M, (c) 10^{-2} M. Perspective view AFM images, 1 X 1 μm with the grey z-scale (height) range as indicated on the images.

Discussion

In every electrochemical cell, each component of the bath is also an additive material that can have specific effects on the deposit that depend on plating conditions. Boric acid, a necessary component of many nickel electroplating solutions, is used to maintain the pH of the electrolyte near the cathode below a level at which basic nickel hydroxide is precipitated. The increase in pH near the cathode that drives the precipitation is produced by the co-deposition of hydrogen from aqueous solutions. Decreasing the metal ion content of the solution changes the ratio of H_2/Ni deposited at the cathode and thus requires an alteration of the boric acid content of the electrolyte to maintain conditions necessary for successful nickel deposition without the formation on $Ni(OH)_2$. These adjustments to the solution chemistry away from conditions normally used for electroforming operations are still well below the diffusion limited current density indicated in Fig. 4. It is therefore reasonable to make limited comparisons between the observed behavior at the cathode in our experiments and the expected behavior during electroforming operations.

Our observation of saccharin on the gold surface supports previous work with other techniques that indicate saccharin will form a condensed layer on the cathode surface[8,9]. We can conclude from our STM observations that the saccharin-Ni and saccharin-Au interaction is much weaker then the Ni-Ni or Ni-Au interaction, at least for the (111) planes since nickel island morphology is not strongly disturbed by the presence of saccharin when growing in a layer-by-layer mode. At more negative deposition potentials, nickel deposits with a 3-D growth mode that is very strongly modified by the same saccharin concentrations. This suggests that saccharin interferes in the process of 3-D crystal growth. To determine whether this is because of an orientation dependence for saccharin-Ni interaction or an unknown geometrical factor will require additional STM experiments with substrates of different orientations.

The observed transition from an increased roughness to a decreased roughness in deposits formed with saccharin present has not previously been reported. One possible explanation for the initial roughening of the nickel stems from the high level of orientation of the polycrystalline gold film substrate used for the experiments. Evaporated gold films naturally have a strong (111) fiber texture with individual grains rotated randomly about the surface normal. The individual gold grains frequently have large (111) terraces at their apexes with an area that depends on the thermal history of the film. Changing the size of these terraces by heat treatment or depositing nickel on a less crystalline material would likely change the nucleation and growth behavior of the initial 3-D nuclei and provide an indication of whether the initial roughening was produced by stress or other property unique to growth on Au(111) terraces at the crystalline interface of the nickel and gold.

Intentionally Left Blank

Conclusion

A commercial SPM system was adapted to image continuously the same location on an electrode surface during the electrodeposition of thin nickel films. In dilute nickel Watts solutions, a relatively high boric acid content is required for producing a uniform electroplate for scanning probe experiments. The hypothesis that saccharin decreases grain size in nickel electroplating by decreasing nickel surface mobility during electrodeposition was shown to be incorrect, at least at the low deposition rates examined. Saccharin can be imaged by STM on Au(111) terraces under conditions where nickel begins to deposit but with a very low imaged height of 0.05 nm. The saccharin that was imaged under these conditions consisted of discrete patches without a resolved packing order. Saccharin initially increases the roughness of electrodeposited nickel prior to developing a smoothing effect compared to nickel deposited without saccharin on polycrystalline gold films. During this roughening period the nickel film morphology is 'spiky' and maintains a more positive skewness value than a nickel film produced without saccharin until the film is approximately 200 nm thick. Both of these effects are more apparent at higher saccharin concentrations. Thicker nickel films, up to at least 1200 nm, have surface feature sizes that decrease with increasing saccharin concentration. This behavior is consistent with the grain-refining effect observed for saccharin in bulk electroplated nickel.

Intentionally Left Blank

References

1. L. Oniciu and L. Muresan, "Some fundamental aspects of leveling and brightening in metal electrodeposition," *Journal of Applied Electrochemistry* **21** (7), 565-574 (1991)

2. Edward B. Saubestre, "The chemistry of bright nickel plating solutions," *Plating*, 1219-1227 (1958)

3. J. Edwards, M. J. Levett, "Radiotracer Study of Addition Agent Behavior: 5—Further Results for Thiourea, p-Toluenesulphonamide and Saccharin," *Transactions of the Institute of Metal Finishing* **14**, 147-156 (1964)

4. T. C. Franklin, "Some mechanisms of action of additives in electrodeposition processes," *Surface and Coatings Technology* **30**, 415-428 (1987)

5. F.A. Moller, O.M. Magnussen, and R.J. Behm, "Two-Dimensional Needle Growth of Electrodeposited Ni on Reconstructed Au(111)," *Physical Review Letters* **77** (15), 3165-3168 (October 1996)

6. FA Moller, J Kintrup, A Lachenwitzer, O. M. Magnussen, and R. J. Behm, "*In situ* STM study of the electrodeposition and anodic dissolution of ultrathin epitaxial Ni films on Au(111)," *Physical Review B* (Condensed Matter) **56** (19), 12506-12518 (1997)

7. A. Lachenwitzer and O.M. Magnussen, "Electrochemical Quartz Crystal Microbalance Study on the Kinetics of Nickel Monolayer and Multilayer Electrodeposition on (111)-Oriented Gold Films," *Journal of Physical Chemistry B* **104** (31), 7424-7430 (2000)

8. V. Ivanova and C. Buess-Herman, "Adsorption of saccharin on Au(111) single crystals," *Journal of Electroanalytical Chemistry* **552**, 45-51 (2003)

9. T Osaka, T Sawaguchi, F Mizutani, T. Yokoshima, M. Takai, Y. Okinaka, "Effects of Saccharin and Thiourea on Sulfur Inclusion and Coercivity of Electroplated Soft Magnetic CoNiFe Film," *Journal of the Electrochemical Society* **146** (9), 3295-3299 (1999)

Intentionally Left Blank

Distribution

5	MS9161	D. Dibble	08761
3	MS9401	J. Kelly	08753
1	MS9161	D. Medlin	08761
1	MS9161	K. McCarty	08761
1	MS9161	N. Bartelt	08761
1	MS9403	A. Morales	08762
1	MS9403	N. Yang	08773
1	MS9401	G. Cardinale	08753
1	MS9401	A. Talin	08751
1	MS9403	G. Lucadamo	08773
1	MS9409	S. Goods	08754
1	MS9401	M. Losey	08753
1	MS9042	S. Griffiths	08752
1	MS1415	S. Hearne	01112
3	MS9018	Central Technical File	08945-1
1	MS0899	Technical Library	09616
1	MS9021	Classification Office, 8511 for Technical Library DOE/OSTI via URL	
1	MS 0323	D. Chavez, LDRD Office	01011

Intentionally Left Blank